CHEMISTRY OF MATERIALS
Article

Chem. Mater. **2010,** *22,* 789–798 789
DOI:10.1021/cm901423g

$SrCo_{0.95}Sb_{0.05}O_{3-\delta}$ as Cathode Material for High Power Density Solid Oxide Fuel Cells[†]

Ainara Aguadero,*[,‡] José Antonio Alonso,[‡,§] Domingo Pérez-Coll,[⊥] Cristina de la Calle,[‡] María Teresa Fernández-Díaz,[||] and John B. Goodenough[§]

[‡]*Instituto de Ciencia de Materiales de Madrid, CSIC, Cantoblanco, E-28049 Madrid, Spain,* [§]*Texas Materials Institute, ETC 9.102, The University of Texas at Austin, Austin, Texas, 78712,* [⊥]*Instituto de Cerámica y Vidrio, CSIC, Cantoblanco, E-28049 Madrid, Spain, and* [||]*Institute Laue-Langevin 156X, F-38042 Grenoble Cedex 9, France*

Received May 25, 2009. Revised Manuscript Received July 27, 2009

The title compound has been selected from the $SrCo_{1-x}Sb_xO_{3-\delta}$ series for its enhanced electronic conductivity, as high as 500 S cm^{-1} at 400 °C, and tested in a single cell as a cathode material for solid oxide fuel cells (SOFC). The characterization of this oxide included X-ray (XRD) and "in situ" temperature-dependent neutron powder diffraction (NPD) experiments, thermal analysis, and impedance spectroscopy. In the test cell, the electrodes were supported on a 300 μm thick pellet of the electrolyte $La_{0.8}Sr_{0.2}Ga_{0.83}Mg_{0.17}O_{3-\delta}$ (LSGM) with Sr_2MgMoO_6 as the anode and $SrCo_{0.95}Sb_{0.05}O_{3-\delta}$ as the cathode. The test cells gave a maximum power density of 0.511 and 0.618 W/cm^2 for temperatures of 800 and 850 °C, respectively, with pure H_2 as fuel and air as oxidant. In the 100−700 °C range, $SrCo_{0.95}Sb_{0.05}O_{3-\delta}$ adopts a tetragonal superstructure of perovskite with $a = a_0$, $c = 2a_0$ ($a_0 \approx 3.9$ Å) defined in the *P*4/*mmm* space group containing two inequivalent Co positions. Sb atoms are randomly distributed at Co2 positions, whereas Co1 sites do not apparently contain Sb. Flattened and elongated $(Co,Sb)O_6$ octahedra alternate along the *c* axis sharing corners in a three-dimensional array (3C-like structure). This material experiences a phase transition from the tetragonal superstructure to a simple cubic perovskite between 700 and 850 °C, probably associated with the endothermic peak observed at 816 °C in the DTA curve. This phase transition is related to the disordering of oxygen vacancies from the three available positions in the tetragonal structure to a single oxygen site in the cubic unit cell with an average thermal factor and occupancy. This structure is stable up to 930 °C; at this temperature the oxygen stoichiometry is 2.46(4). The good performance of this material as a cathode is related to its mixed electronic-ionic conduction (MIEC) properties, which can be correlated to the investigated structural features: the Co^{3+}/Co^{4+} redox energy at the top of the O 2p bands accounts for the excellent electronic conductivity, which is favored by the corner-linked perovskite network. The considerable number of oxygen vacancies, with the oxygen atoms showing high displacement factors (4−6 Å^2 in the 700−850 °C range), suggests a significant ionic mobility. Additionally, this cathode material exhibits an extremely low electrode polarization resistance, below 0.1 Ω cm^2 in the 750−800 °C range. The thermal expansion is compatible with the electrolyte and the nonreconstructive tetragonal-to-cubic transition does not involve an abrupt change in unit-cell volume, which increases smoothly over the entire temperature interval up to 930 °C.

1. Introduction

One of the major goals in solid oxide fuel cell (SOFC) technology is the reduction of the operating temperature to intermediate values (550−850 °C) in order to improve the compatibility of the different constituent materials and decrease the operation costs. Therefore, the development of new mixed ionic-electronic conductors as electrodes with sufficient conductivity at moderate temperatures is a prime target. The high-temperature cubic phase of $SrCoO_{3-\delta}$ is a promising material because of its high electrical conductivity and oxygen permeation flux.[1−3] However, this phase is not stable below 900 °C where a 3C-cubic to 2H-hexagonal phase transition takes place when the sample is slowly cooled. Further studies demonstrated that this hexagonal phase is, in fact, slightly Co deficient, with a stoichiometry $Sr_6Co_5O_{15}$. On the other hand, $SrCoO_{3-\delta}$ is able to adopt very different structural phases as a function of the oxygen partial

---

[†] Accepted as part of the 2010 "Materials Chemistry of Energy Conversion Special Issue".

*Corresponding author. E-mail: ainara.aguadero@icmm.csic.es.

(1) Deng, Z. Q.; Yang, W. S.; Liu, W.; Chen, C. S. *J. Solid State Chem.* **2006**, *179*, 362.
(2) Takeda, Y.; Kanno, R.; Takada, T.; Yamamoto, O.; Takano, M.; Bando, Y. *Z. Anorg. Allg. Chem.* **1986**, *540−541*, 259.
(3) De la Calle, C; Aguadero, A.; Alonso, J. A.; Fernández-Díaz, M. T. *Solid State Sci.* **2008**, *10*, 1924.

pressure, temperature, and cooling rates as has been broadly studied by different authors. [4-9]

The stabilization of a 3C perovskite framework in the $SrCoO_{3-\delta}$ system has been a widely used strategy to obtain an adequate mixed ionic-electronic conductor to be used as a cathode in intermediate-temperature solid oxide fuel cells. For this purpose, several substitutions have been performed in either the Sr (Ba, La, Sm)[10] or the Co (Sc, Fe, Ni, etc.)[11,12] positions, or in both. The most widely used derivatives of $SrCoO_{3-\delta}$ are $Ba_{0.5}Sr_{0.5}Co_{0.8}Fe_{0.2}O_{3-\delta}$ (BSCF)[13,14] and $SrCo_{0.8}Fe_{0.2}O_{3-\delta}$ (SCF) because of their high oxygen fluxes and favorable oxygen-reduction performance at temperatures $\geq$600 °C.[15,16] However, at the SOFC operating temperatures these materials display a relatively low electronic conductivity ($\sim$ 35 S cm^{-1}) [17] compared to that expected for cathode materials ($\sim$ 100 S cm^{-1}), which might be one of the problems responsible for their low performance at temperatures below 600 °C.[18,19] Their thermal stability and polarization resistances must be improved before they can be considered for positive electrodes in a SOFC. Moreover, some studies have proved that the cubic BSCF is unstable in air,[20] and in the presence of CO_2 at intermediate temperatures ($\sim$ 500 °C); it forms carbonates very detrimental for the electrochemical performance.[21,22] Moreover, the structural instability increases with the barium concentration[23] and the oxygen permeability and electrical conductivity increase with decreasing concentrations of the substituent cations in Sr and Co positions.[24,25]

In a previous work, we have stabilized a 3C perovskite phase by doping the $SrCoO_{3-\delta}$ system with low Sb contents in $SrCo_{1-x}Sb_xO_{3-\delta}$ (x = 0.05, 0.1, 0.15, and 0.2). The stabilization of a tetragonal *P4/mmm* structure was obtained with x = 0.05−0.15.[26] The "in situ" thermal evolution of the crystal structure was followed by neutron powder diffraction measurements for the x = 0.1 compound.[27] At x = 0.2, a phase transition takes place and the room-temperature material is defined in the cubic $Pm\bar{3}m$ space group. The Sb-doped compounds present high thermal stability without abrupt changes in the expansion coefficient and a great enhancement of the electrical conductivity compared to the pristine $SrCoO_{3-\delta}$ at low and intermediate temperatures ($T \leq 800$ °C). As predicted, the sample with lower doping level (x = 0.05) displayed the highest conductivity value, over 160 S·cm^{-1} in the usual working conditions of a cathode in a SOFC (650−900 °C), and the lowest area specific resistance (ASR) values ranging from 0.009 to 0.23 Ω cm^2 in the 600−900 °C temperature interval with $Ce_{0.8}Nd_{0.2}O_{2-\delta}$ as electrolyte. For $SrCo_{0.95}Sb_{0.05}O_{3-\delta}$, a maximum power density higher than 300 mW cm^{-2} at 700 °C was estimated, assuming an electrolyte thickness of 200 μm in a ceria-based SOFC and typical values of 0.85 V and 0.1 Ω cm^2 for the open-circuit potential (OCP) and the anode polarization, respectively.

In the present study, the $SrCo_{0.95}Sb_{0.05}O_{3-\delta}$ compound has been deeply analyzed as a potential SOFC cathode. For this purpose, the in situ evolution of the crystal structure of $SrCo_{0.95}Sb_{0.05}O_{3-\delta}$ has been followed under the usual working conditions of a cathode in a SOFC (in air from 25 to 950 °C). In addition, the polarization resistance and chemical compatibility of the compound with $La_{0.8}Sr_{0.2}Ga_{0.8}Mg_{0.2}O_{3-\delta}$ (LSGM) electrolyte has been tested in an Anode/300 μm thick LSGM/$SrCo_{0.95}Sb_{0.05}O_{3-\delta}$ single cell. The obtained results are remarkably good, leading to power densities higher than 600 mW cm^{-2} at 850 °C.

2. Experimental Section

2.1. Synthesis, Structural, and Thermal Characterization. $SrCo_{0.95}Sb_{0.05}O_{3-\delta}$ was prepared via a nitrate-citrate route. The starting materials Sb_2O_3, $Sr(NO_3)_2$, and $Co(NO_3)_2\cdot 6H_2O$ of analytical grade were dissolved under stirring in 250 mL of 10% citric-acid aqueous solution containing some drops of HNO_3. The solution was slowly evaporated, leading to an organic resin that was dried at 120 °C and decomposed at temperatures up to 600 °C for 12 h. The sample was then heated at 900 °C for 12 h and at 1000 °C for 24 h with intermediate grinding. After the thermal treatments, the sample was cooled in the furnace at 5 °C/min approximately. The reaction product was characterized by X-ray diffraction (XRD) for phase identification and to assess phase purity. The characterization was performed with a Bruker-axs D8 diffractometer (40 kV, 30 mA) in Bragg−Brentano reflection geometry with Cu Kα radiation (λ = 1.5418 Å).

---

(4) Harrison, W.; Hedwood, S. L.; Jacobson, A. J. *J. Chem. Soc., Chem. Commun.* **1995**, 1953.

(5) Grenier, J. G.; Ghodbane, S.; Demazeau, G.; Pouchard, M.; Hagenmuller, P. *Mater. Res. Bull.* **1979**, *14*, 831.

(6) Battle, P. D.; Gibb, T. C.; Steel, A. T *J. Chem. Soc., Dalton Trans.* **1987**, 2359.

(7) Battle, P. D.; Gibb, T. C. *J. Chem. Soc., Dalton Trans.* **1987**, 667.

(8) Battle, P. D.; Gibb, T. C.; Steel, A. T. *J. Chem. Soc., Dalton Trans.* **1988**, 83.

(9) Vashook, V. V.; Zinkevich, M. V.; Zonov, Y. G. *Solid State Ionics* **1999**, *116*, 129.

(10) Nagai, T.; Ito, W.; Sakon, T. R. *Solid State Ionics* **2007**, *177*, 3433.

(11) Deng, Z. Q.; Liu, W.; Chen, C. S.; Lu, H.; Yang, W. S. *Solid State Ionics* **2004**, *170*, 187.

(12) Zeng, P.; Ranj, R.; Chen, Z.; Zhou, W.; Gu, H.; Shao, Z.; Liu, S. *J. Alloys Compd.* **2008**, *455*, 465.

(13) Shao, Z. P.; Haile, S. M. *Nature* **2004**, *431*, 170.

(14) Zhou, W.; Ran, R.; Shao, Z. *J. Power Sources* **2009**No. doi: 10.1016/j.jpowsour.2009.02.069.

(15) Baumann, F. S.; Fleig, J.; Habermeir, H.-U.; Maier, J. *Solid State Ionics* **2006**, *177*, 3187.

(16) Lim, Y. H.; Lee, J.; Yoon, J. S.; Kim, C. E.; Hwang, H. J. *J. Power Sources* **2007**, *171*, 79.

(17) Wei, B.; Lü, Z.; Huang, X.; Miao, J.; Sha, X.; Xin, X.; Su, W. *J. Eur. Ceram. Soc* **2006**, *26*, 2827.

(18) Peña-Martínez, J.; Marrero-Lopez, D.; J Ruiz-Morales, C.; Buergler, B. E.; Nuñez, P.; Gauckler, L. J. *Solid State Ionics* **2006**, *177*, 2143.

(19) Shao, Z. P.; Haile, S. M. *Nature* **2004**, *431*, 170.

(20) Svarcova, S.; Wiik, K.; Tolchard, J.; Bouwmeester, H. J. M.; Grande, T. *Solid State Ionics* **2008**, *178*, 1787.

(21) Arnold, M.; Wang, H.; Feldhoff, A. *J. Membr. Sc.* **2007**, *193*, 44.

(22) Yang, A.; Cheng, M.; Dong, Y.; Yang, W.; Maragou, V.; Song, S.; Tsiakaras, P. *Appl. Catal., B* **2006**, *66*, 64.

(23) Yang, A.; Liu, B.; Dong, Y.; Tian, Z.; Wang, D. M.; Cheng *Appl. Catal., B* **2008**, *80*, 24.

(24) Teraoka, Y.; Zhang, H.-M.; Furukawa, S.; Yamazoe, N. *Chem. Lett.* **1985**, 1743.

(25) Wiik, K.; Aasland, S.; Hansen, H. L.; I. Tangen, L.; Odegard, R. *Solid State Ionics* **2002**, *152*−*153*, 675.

(26) Aguadero, A.; De la Calle, C.; Alonso, J. A.; Escudero, M. J.; Fernandez-Díaz, M. T.; Daza, L. *Chem. Mater.* **2007**, *19*, 6437.

(27) Aguadero, A.; Pérez-Coll, D.; De la Calle, C.; Alonso, J. A.; Escudero, M. J.; Daza, L. *J. Power Sources* **2008**No. DOI 10.1016/j.jpowsour.2008.12.138.

Neutron powder diffraction (NPD) data were collected in the diffractometer D1A at the Institut Laue-Langevin, Grenoble. The high intensity mode ($\Delta d/2 \geq 2 \times 10^{-3}$) was selected, with a neutron wavelength $\lambda = 1.91$ Å within the angular 2θ range from 5 to 165°. About 2 g of the sample was contained in a quartz tube open to ambient atmosphere and placed in the isothermal zone of a furnace with a vanadium resistor operating under vacuum ($P_{O_2} \approx 1 \times 10^{-6}$ Torr). The measurements were carried out in air at 100, 200, 350, 500, 700, 850, 900, and 930 °C. The collection time was 3 h per pattern. The diffraction data were analyzed by the Rietveld method with the FULLPROF program[28] and the use of its internal tables for scattering lengths. The line shape of the diffraction peaks was generated by a pseudo-Voigt function. The irregular background coming from the quartz container was extrapolated from points devoid of reflections. In the final run, the following parameters were refined: background points, zero shift, half-width, pseudo-Voigt, and asymmetry parameters for the peak shape, scale factor, and unit-cell parameters. Positional and occupancy factors for oxygen atoms and isotropic thermal factors were also refined for the NPD data. The coherent scattering lengths for Sr, Co, Sb, and O were, 7.02, 2.49, 5.57, and 5.803 fm, respectively.

Differential thermal analysis (DTA) and thermogravimetric (TG) curves in air were simultaneously obtained in a Stanton STA 781 instrument. The temperatures of the peaks were measured with an accuracy of ±1 °C. Analyses were carried out in still air at 10 °C min^{-1} heating/cooling rate. The sample and reference were situated in platinum crucibles, and α-Al_2O_3 was the inert reference. The thermogravimetric curve in reducing conditions of about 50 mg of powder was recorded in a Mettler Toledo TG50 instrument in the 35−900 °C temperature range under a H_2(5%)/N_2(95%) flow (100 mL min^{-1}).

Scanning electron microscopy (Hitachi S-2500) measurements were performed on the studied cells to analyze the good adherence and microstructure of the components.

2.2. Electrode Polarization by Impedance Spectroscopy. Impedance spectroscopy measurements were performed in air under open-circuit potential (OCP) conditions in a symmetrical configuration to extract the corresponding values of electrolyte and electrode contributions. For this purpose, a dense electrolyte pellet of LSGM (Praxair) was prepared by pressing the powder in a 15-mm die and sintering at 1500 °C for 10 h. The density of the pellet was calculated from the mass and geometrical volume. The powder of $SrCo_{0.95}Sb_{0.05}O_{3-\delta}$ was ball-milled with YSZ balls in ethanol to break the agglomerates. Then the dried powder was mixed with a binder (Decoflux), symmetrically painted over the electrolyte, and calcined at 900 °C for 4 h, obtaining circular 5.50 mm diameter electrodes. To obtain equipotential conditions, Pt paste was applied over the cathode material, and the sample was calcined again to 900 °C for 1 h. Impedance spectroscopy in air and OCP was then performed in potentiostatic mode, decreasing the temperature from 900 to 500 °C, with an excitation voltage of 50 mV in the range of 1×10^{6} to 1×10^{-2} Hz.

2.3. Fuel Cell Tests. Single-cell tests were made on electrolyte-supported cells with $La_{0.8}Sr_{0.2}Ga_{0.83}Mg_{0.17}O_{3-\delta}$ (LSGM) as the electrolyte. LSGM pellets of 20 mm diameter were sintered at 1450 °C for 20 h and then polished with a diamond wheel to a thickness of 300 μm. The anode was the double perovskite $Sr_2MgMoO_{6-\delta}$ (SMMO) prepared by a sol−gel technique as described elsewhere;[29] $La_{0.4}Ce_{0.6}O_{2-\delta}$ (LDC) was used as a buffer layer between the anode and the electrolyte in order to prevent the interdiffusion of ionic species between perovskite and electrolyte. Inks of LDC, SMMO and $SrCo_{0.95}Sb_{0.05}O_{3-\delta}$ (SCSO) were prepared with a binder (V-006 from Heraeus). LDC ink was screen-printed onto one side of the LSGM disk followed by a thermal treatment at 1300 °C in air for 1 h. SMMO was subsequently screen printed onto the LDC layer and fired at 1275 °C in air. SCSO was finally screen printed onto the other side of the disk and fired at 1000 °C for 1 h. The working electrode area of the cell was 0.24 cm^2 (0.6 × 0.4 cm). Reference electrodes of the same materials as the working electrodes were used to monitor the overpotentials of the cathode and anode in the cell configuration.[30,31] Pt gauze with a small amount of Pt paste in separate dots was used as current collector at both the anodic and the cathodic sides for ensuring electrical contact. The cells were tested in a vertical tubular furnace at 750, 800, and 850 °C; the anode side was fed with a flow of pure H_2 (20 mL/min), whereas the cathode worked in an air flow of 100 mL/min.

The fuel-cell tests were performed with an EG&G potentiostat/galvanostat by changing the voltage of the cell from the OCP to 0.3 V, with steps of 0.030 V, holding 10 s at each step. Current density was calculated by the recorded current flux through the effective area of the cell (0.24 cm^2). The electrolyte voltage drop was calculated from the electrolyte conductivity obtained by a.c. impedance spectroscopy in air. The stability of the cell was evaluated by performing the fuel-cell test from the OCP to 0.3 V in 50 cycles.

3. Results

3.1. Crystallographic Characterization. $SrCo_{0.95}Sb_{0.05}O_{3-\delta}$ was obtained as a pure, well-crystallized perovskite phase; Figure 1 shows the XRD pattern at RT, indexed in a tetragonal unit cell with $a = b \approx 3.87$ Å, $c \approx 3.90$ Å based on the aristotype ($a_0 \approx 3.90$ Å) with a small axial deformation. As shown for $SrCo_{0.9}Sb_{0.1}O_{3-\delta}$,[26] the NPD diagram collected at RT showed a superstructure with doubled c-axis, as $a = b \approx a_0$, $c \approx 2a_0$. The NPD patterns collected between 100 and 700 °C for $SrCo_{0.95}Sb_{0.05}O_{3-\delta}$ were correctly refined in the $P4/mmm$ model derived for $SrCo_{0.9}Sb_{0.1}O_{3-\delta}$.[26] In this perovskite, Sr atoms are placed at $2h$ (1/2, 1/2, z) sites; Co and Sb were initially distributed over the $1a$ (0, 0, 0) (labeled Co1) and $1b$ (0, 0, 1/2) (labeled (Co, Sb)2) sites, and the three kinds of oxygen atoms, O1 at $2f$ (1/2, 0, 0), O2 at $2g$ (0, 0, z) and O3 at $2e$ (1/2, 0, 1/2). After the refinement, the Sb occupancy at $1a$ sites converged to zero; all the Sb content was concentrated at $1b$ positions. In the final run, the occupancy factors for the three types of oxygen atoms were also refined. For O1, the occupancy factors converged to a value slightly higher than unity (e.g., 1.061(1)), which suggests a full occupancy for this atom. For O2 and O3 there is indeed an oxygen deficiency. For instance, at 100 °C we obtained a crystallographic formula $Sr(Co_{0.9}Sb_{0.1})O_{2.72(4)}$ from the NPD refinement. Figure 2a illustrates the goodness of the fit for the 100 °C patterns;

---

(28) Rodríguez-Carvajal, J. *Physica B* **1993**, *192*, 55.

(29) Huang, Y.-H.; Dass, R. I.; Xing, Z.-L.; Goodenough, J. B. *Science* **2006**, *312*, 254.

(30) Wan, J.-H.; Yan, J.-Q.; Goodenough, J. B. *J. Electrochem. Soc.* **2005**, *152*, A1511.

(31) Feng, M.; Goodenough, J. B.; Huang, K.; Milliken, C. *J. Power Sources* **1996**, *63*, 47.

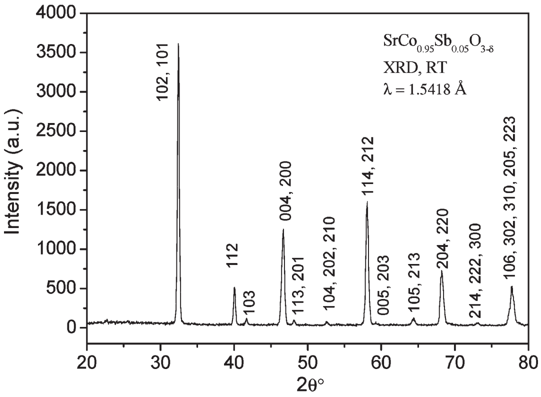

Figure 1. X-ray diffraction diagram of $SrCo_{0.95}Sb_{0.05}O_{3-\delta}$, tentatively indexed in a simple tetragonal unit cell with $a \approx 3.87$ Å and $c \approx 3.90$ Å.

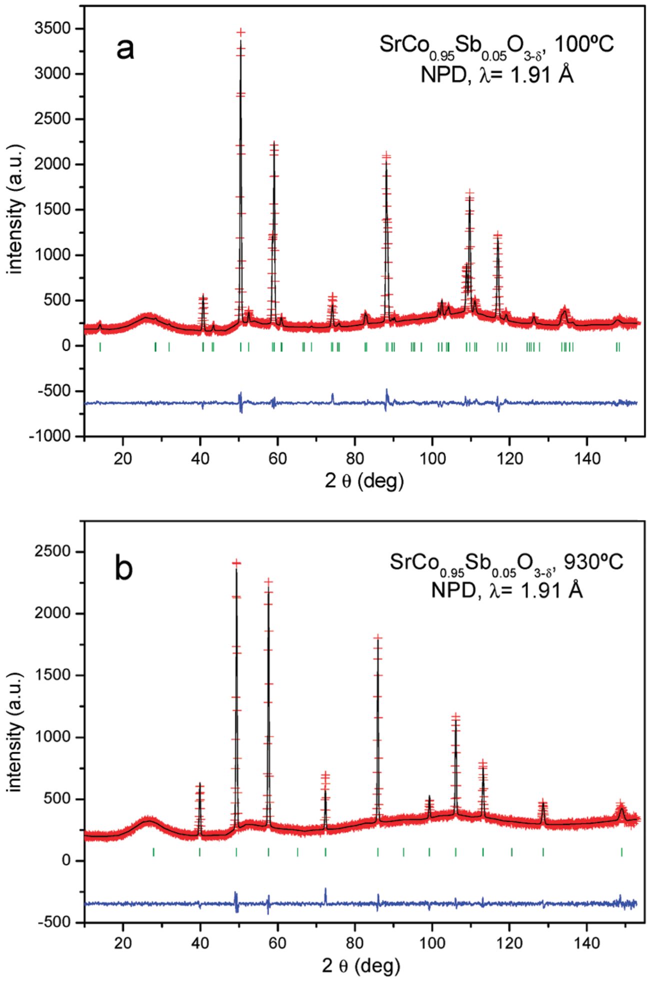

Figure 2. Observed (crosses), calculated (full line), and difference (at the bottom) NPD profiles for $SrCo_{0.95}Sb_{0.05}O_{3-\delta}$ at (a) 100 °C, refined in the $P4/mmm$ space group, and (b) 930 °C, refined in the cubic $Pm\bar{3}m$. The vertical markers correspond to the allowed Bragg reflections. The irregular background is due to the quartz container.

Table 1 lists the final structural parameters and discrepancy factors obtained from 100 to 700 °C NPD data.

The NPD diagrams collected above 700 °C showed the disappearance of the superstructure reflections arising from the doubling of the unit cell along the *c*-direction; all the peaks could be indexed in a simple-cubic perovskite unit cell with $a = a_0$. The structure was modeled in the space group $Pm\bar{3}m$ with Sr at 1*b* (1/2, 1/2, 1/2) positions, Co and Sb distributed at random over the 1*a* (0,0,0) positions and a single type of oxygen atom at 3*d* (1/2, 0, 0) sites. The structure was successfully refined in this model at 850, 900, and 930 °C; the refinement of the occupancy factors of the oxygen position unveil a serious oxygen deficiency that progressively increases with temperature, reaching the composition $Sr(Co_{0.9}Sb_{0.1})O_{2.46(2)}$ at 930 °C. Figure 2b illustrates the goodness of the fit for the 930 °C diagram. Table 2 contains the main structural parameters of the cubic structures at 850, 900, and 930 °C. Tables 3 and 4 list the main interatomic distances for the different temperatures. Figure 3a and 3b display the thermal variation of the unit-cell parameters and volume, respectively, showing the transition from a low-temperature tetragonal superstructure to the high-temperature simple-cubic symmetry. The transition temperature is in the 700−850 °C range. Figure 3c shows the evolution of the oxygen contents, refined from NPD data. Figure 4 shows the crystal structures of the tetragonal and cubic phases. The anisotropic thermal vibrations have been introduced to describe the thermal motions of the oxygen atoms. For O1, the anisotropic refinement leads to negative values of one of the semi-axes of the thermal ellipsoids, so it was described as isotropic. For O2 and O3 they have successfully been described as anisotropic. In both cases, the largest thermal motions are perpendicular to the Co−O bonds, as expected. Figure 5 graphically shows the orientation of the ellipsoids viewed along the [001] direction, suggesting a dynamical tilting of the $(Co,Sb)2O_6$ octahedra. The possibility of a static tilting of the octahedra along the *c* axis has also been considered. However, this tilting effect would forcedly lead to superstructures with larger *a* and *b* unit-cell parameters, giving rise to superstructure reflections which have not been observed in the NPD patterns. Typically, the $a^0a^0c^+$ or $a^0a^0c^-$ tilting systems would be described in the space groups $P4/mnc$ and $I4/m$, respectively, which would require $\sqrt{2}a_0 \times \sqrt{2}a_0 \times 2a_0$ unit cells (double in size from the one considered at present, $a_0 \times a_0 \times 2a_0$); trial refinements in the corresponding structural models were totally unsuccessful at describing the crystal structure, leading to poor agreement factors and leaving several observed reflections unexplained because of the extinction conditions of the mentioned space groups.

3.2. Thermal Analysis. The oxygen content of the sample was determined by thermal analysis under reducing conditions and by neutron-diffraction refinement of the oxygen occupancy. Figure 6a shows the TG and DTG curves of $SrCo_{0.95}Sb_{0.05}O_{3-\delta}$ obtained in a 5% H_2 flow. A weight loss of 16.06% is observed between 100 and 900 °C. After the sample was cooled, the final product was identified by XRD as a mixture of SrO, Co metal and Sb_2O_3. From the observed weight loss, the oxygen stoichiometry of the starting sample is 2.75(2), in excellent agreement with the 2.72(4) oxygen content determined by neutron diffraction at 100 °C.

Figure 6b shows the thermal analysis, TG and DTA curves for $SrCo_{0.95}Sb_{0.05}O_{3-\delta}$ carried out in air between

Table 1. Unit-cell, Positional, And Displacement Parameters for $SrCo_{0.95}Sb_{0.05}O_{3-\delta}$ in the Tetragonal *P4/mmm* (No. 123) Space Group, $Z = 2$, from NPD Data at 100, 200, 350, 500, 600, and 700 °C

	T (°C)					
	100	200	350	500	600	700
a (Å)	3.87222(3)	3.87880(3)	3.89034(3)	3.90748(3)	3.91977(4)	3.93344(4)
c(Å)	7.79702(8)	7.80544(8)	7.82582(8)	7.86438(8)	7.8837(1)	7.8941(1)
V(Å^3)	116.911(2)	117.434(2)	118.442(2)	120.077(2)	121.130(2)	122.144(2)
			Sr 2*h* (1/2, 1/2, *z*)			
z	0.2615(3)	0.2608(3)	0.2602(3)	0.2602(3)	0.2601(4)	0.2582(4)
B (Å^2)	1.04(5)	1.24(6)	1.49 (6)	1.82 (6)	2.17(7)	2.39(6)
f_{occ}	1.0	1.0	1.0	1.0	1.0	1.0
			Co1 1*a* (0, 0, 0)			
B (Å^2)	0.4(2)	0.2(2)	0.3(2)	0.4(2)	0.7(2)	1.4(3)
f_{occ}(Co)	1.0	1.0	1.0	1.0	1.0	1.0
			(Co,Sb)2 1*b*(0, 0, 1/2)			
B (Å^2)	2.1(3)	1.8(3)	1.4(3)	2.5(3)	2.5(4)	3.1(5)
f_{occ}(Co)	0.9	0.9	0.9	0.9	0.9	0.9
f_{occ}(Sb)	0.1	0.1	0.1	0.1	0.1	0.1
			O1 2*e* (1/2, 0, 0)			
B (Å^2)	1.01(6)	1.12(7)	1.30(7)	1.74(7)	2.15(9)	3.0(1)
f_{occ}	1.0	1.0	1.0	1.0	1.0	1.0
			O2 2*g* (0, 0, *z*)			
z	0.7699 (4)	0.7695(4)	0.7677(4)	0.7709(5)	0.7699(6)	0.7672(7)
B_{eq} (Å^2)^a	1.8(2)	2.0(2)	2.0(2)	3.2(2)	3.3(3)	3.9(4)
$\beta_{11} = \beta_{22}$	0.040(3)	0.041(3)	0.046(3)	0.065(4)	0.068(5)	0.082(7)
β_{33}	0.0059(6)	0.0061(7)	0.0073(8)	0.0082(7)	0.0078(9)	0.008(1)
f_{occ}	0.96(2)	0.94(2)	0.92(2)	0.94(2)	0.89(2)	0.84(3)
			O3 2*f* (1/2, 0, 1/2)			
B_{eq} (Å^2)^b	5.7 (2)	5.4(2)	5.4(2)	6.8(2)	6.6(3)	6.4(3)
β_{11}	0.056(5)	0.047(5)	0.041(5)	0.045(5)	0.050(5)	0.037(5)
β_{22}	0.129(9)	0.125(9)	0.122(9)	0.136(9)	0.13(1)	0.11(1)
β_{33}	0.026(2)	0.025(1)	0.025(1)	0.033(2)	0.035(2)	0.041(2)
f_{occ}	0.764(9)	0.768(9)	0.779(9)	0.777(9)	0.78 (1)	0.80(1)
			reliability factors			
χ^2	1.97	1.88	1.56	2.1	1.41	1.30
R_{Bragg}(%)	4.82	4.90	4.26	4.01	4.15	4.05

[a] Anisotropic thermal factors $\beta_{11} = \beta_{22} \neq \beta_{33}, \beta_{12} = \beta_{13} = \beta_{23} = 0$. [b] Anisotropic thermal factors $\beta_{11} \neq \beta_{22} \neq \beta_{33}, \beta_{12} = \beta_{13} = \beta_{23} = 0$.

Table 2. Unit-Cell, Positional, and Displacement Parameters for $SrCo_{0.95}Sb_{0.05}O_{3--\delta}$ in the Cubic $Pm\overline{3}m$ (No. 221) Space Group, $Z = 1$, at 850, 900, and 930 °C from In situ NPD Data

	T (°C)		
	850	900	930
a (Å)	3.95479(4)	3.96033(4)	3.96368(4)
V (Å^3)	61.854(1)	62.114(1)	62.272(1)
		Sr 1*b* (1/2, 1/2, 1/2)	
B (Å^2)	3.0(1)	3.2(1)	3.32(9)
f_{occ}	1.0	1.0	1.0
		Co, Sb 1*a* (0, 0, 0)	
B (Å^2)	2.4(2)	2.8(2)	2.6(2)
f_{occ}(Co)	0.95	0.95	0.95
f_{occ}(Sb)	0.05	0.05	0.05
		O 3*d* (1/2, 0, 0)	
B_{eq} (Å^2)^a	4.8(1)	5.0(1)	5.11(9)
β_{11}	0.049(3)	0.053(3)	0.052(3)
$\beta_{22} = \beta_{33}$	0.091(2)	0.094(2)	0.097(2)
f_{occ}	0.84(2)	0.83(2)	0.82 (2)
		reliability factors	
χ^2	2.99	2.46	2.25
R_{Bragg}(%)	1.99	0.89	1.28

[a] Anisotropic thermal factors $\beta_{11} \neq \beta_{22} = \beta_{33}, \beta_{12} = \beta_{13} = \beta_{23} = 0$.

35 and 1000 °C. The TG curve shows an almost linear weight loss while heating the sample up to 260 °C followed by a broad exothermic peak in the DTA curve, probably because of the dehydration and/or decarboxylation of the sample. Subsequently, between 300 and 430 °C a gain of mass of about 0.09% is observed. This gain has been interpreted as an incorporation of lattice oxygen as has been shown by the Rietveld refinement of the oxygen occupancy at 500 °C (Table 1). At higher temperatures, three endothermic peaks at 816, 877, and 908 °C have been observed. These peaks are accompanied by an abrupt weight loss in the TG curve leading to oxygen contents around 2.5; it is related to the tetragonal to cubic transition observed in this temperature range by the NPD measurements. An XRD study of the sample after the thermal analysis experiment gives exactly the same diffraction pattern as the initial compound, confirming the absence of phase segregation or decomposition after the thermal treatment in air.

3.3. Impedance Spectroscopy Results. The electrode performance was first evaluated by impedance spectroscopy in air under OCP conditions with the same electrode on opposite sides of the LSGM electrolyte. Figure 7 shows the impedance spectra obtained at 750, 800, and 850 °C. The series resistance was subtracted from the spectra in order to have an estimation of the electrode polarization as a function of temperature. The results

Table 3. Main Bond Distances (Å) for the Tetragonal $SrCo_{0.95}Sb_{0.05}O_{3-\delta}$ Phase Determined from NPD Data at 100, 200, 350, 500, 600, and 700 °C; Space Group *P4/mmm*

	T (°C)					
	100	200	350	500	600	700
			SrO_{12} polyhedron			
Sr−O1 (×4)	2.812(2)	2.812(2)	2.816(2)	2.829(2)	2.837(2)	2.832(2)
Sr−O2 (×4)	2.7490(3)	2.7529(3)	2.7595 (3)	2.7738(4)	2.7818(5)	2.7886(5)
Sr−O3 (×4)	2.684(2)	2.692 (2)	2.703(2)	2.715(2)	2.724 (2)	2.741(2)
⟨Sr−O⟩	2.748	2.752	2.760	2.773	2.781	2.787
			$(Co,Sb)1O_6$ octahedron			
(Co)1−O1 (×4)	1.9361(0)	1.9394(0)	1.9452(0)	1.9537(0)	1.9599(0)	1.9667(0)
(Co)1−O2 (×2)	1.794(3)	1.799(3)	1.818(4)	1.802(4)	1.814(5)	1.838(6)
⟨(Co)1−O⟩	1.889	1.893	1.903	1.903	1.911	1.924
			$(Co,Sb)2O_6$ octahedron			
(Co,Sb)2−O2 (×2)	2.104(3)	2.104(3)	2.095 (3)	2.130(4)	2.128 (5)	2.109(6)
(Co,Sb)2−O3 (×4)	1.9361(0)	1.9394(0)	1.9452(0)	1.9537(0)	1.9599(0)	1.9667(0)
⟨(Co,Sb)2−O⟩	1.992	1.994	1.995	2.012	2.016	2.014

Table 4. Main Bond Distances (Å) for the Cubic $SrCo_{0.95}Sb_{0.05}O_{3-\delta}$ Phase Determined from NPD Data at 850, 900, and 930 °C; Space Group *Pm$\bar{3}$m*

	T (°C)		
	850	900	930
	SrO_{12} polyhedron		
Sr−O (×12)	2.7964(1)	2.8004(1)	2.8027(1)
	$(Co,Sb)1O_6$ octahedron		
(Co,Sb) −O (×6)	1.9774(1)	1.9802(1)	1.9818(1)

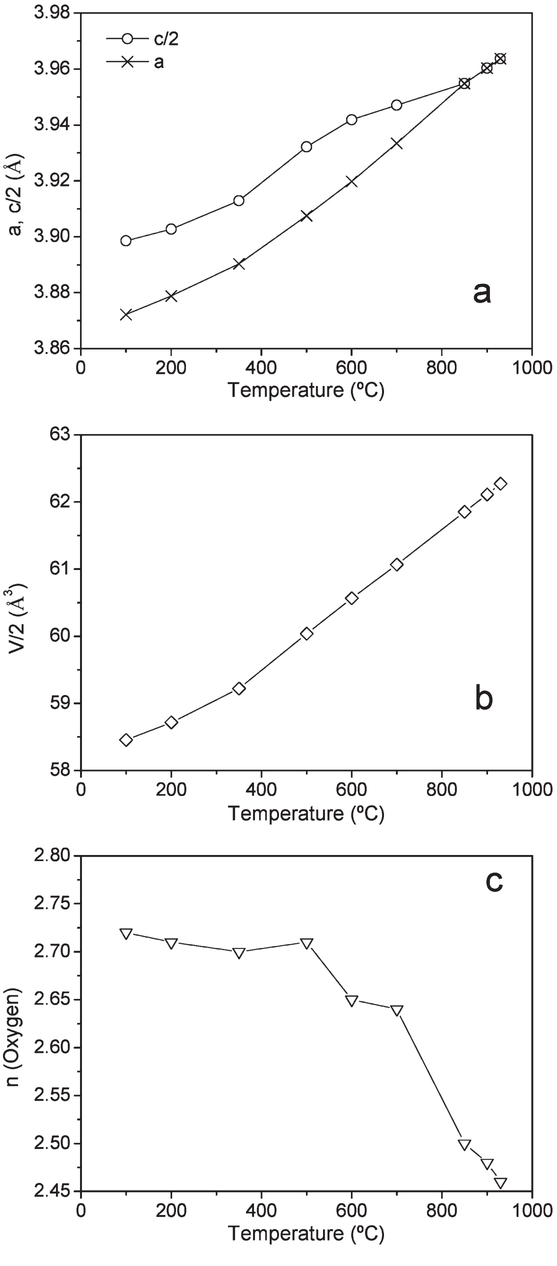

Figure 3. Thermal variation of (a) unit-cell parameters, (b) volume, and (c) oxygen contents of $SrCo_{0.95}Sb_{0.05}O_{3-\delta}$ from in situ NPD data. A phase transition between tetragonal to cubic occurs between 700 and 850 °C.

were also multiplied by the electrode area and 0.5 to account for the contribution of both electrodes. The good performance of $SrCo_{0.95}Sb_{0.05}O_{3-\delta}$ as a cathode with the LSGM electrolyte is evidenced by the low electrode polarization resistance: 0.115, 0.069, and 0.045 Ω cm^2 for temperatures of 750, 800, and 850 °C, respectively (Figure 7). The Arrhenius representation of the electrode polarization resistance shows an activation energy of 0.97 eV in the range of 650−900 °C (Figure 8), which is clearly higher than the electrolyte activation energy (0.62 eV). This higher activation energy could spoil the cathode efficiency at intermediate temperatures; however, the experimental results show polarization values as low as 0.2 Ω cm^2 even at 700 °C. One can determine electrode overpotential values as low as 0.242, 0.135, and 0.082 V for a current flux of 1.2 A/cm^2 and temperatures of 700, 750, and 800 °C, respectively. Figure 9 reveals that the voltage losses of the LSGM electrolyte under similar conditions are 0.387, 0.257, and 0.182 V, respectively, if we assume a thickness of 300 μm. This result indicates that the electrode overpotential is retained lower than the electrolyte loss even at intermediate temperatures, which indicates it will produce good performance when used as the cathode in a SOFC.

3.4. Fuel-Cell Test. The performance of the $SrCo_{0.95}Sb_{0.05}O_{3-\delta}$ cathode was also tested in a single cell using air in contact with the cathode and dry H_2 as a fuel. Figure 10 shows the cathode and anode overpotentials at 800 °C as a function of current density. The overpotential is practically linear for the cathode, whereas there is a deviation from linearity for the anode

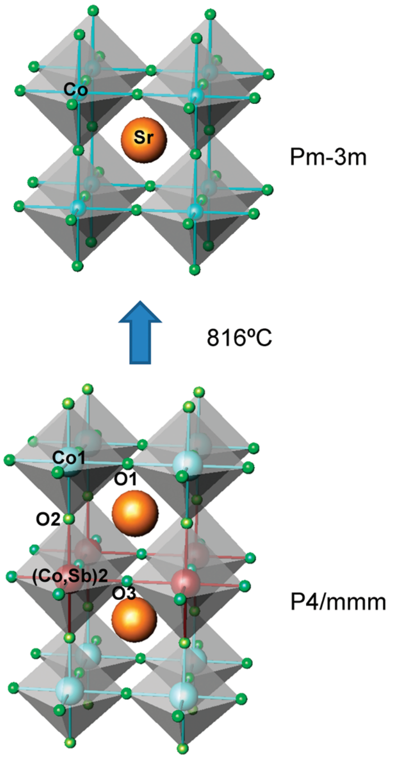

Figure 4. Bottom panel: Tetragonal crystal structure observed for $SrCo_{0.95}Sb_{0.05}O_{3-\delta}$ below 816 °C, where an array of corner-linked $Co1O_6$ octahedra alternates along the *c* axis with layers of $(Co,Sb)2O_6$ octahedra. Top panel: High-temperature structure corresponding to the cubic aristotype.

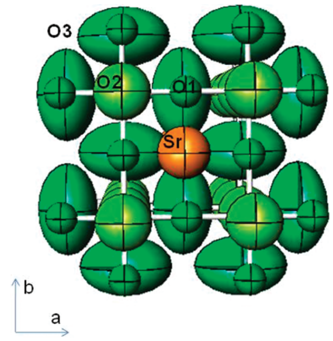

Figure 5. View of the tetragonal crystal structure along the [001] direction showing the orientation of the ellipsoids.

at lower current densities. Moreover, the cathode presents values of overpotential more than 6 times smaller than the anode, whereas the voltage drop in the electrolyte is nearly 3 times larger than the cathode overpotential. Figure 11 shows the voltage of the cell and the power density as a function of the current density for 750, 800, and 850 °C. The nonlinear behavior of the anode overpotential is evidenced in the voltage of the cell for lower current densities. The maximum power densities generated by the cell are 0.328, 0.511, and 0.618 W/cm^2 for temperatures of 750, 800, and 850 °C, respectively. On the other hand, the experimental results of the overpotential in the cathode match well with the electrode polarization resistance obtained by impedance spectroscopy in air and give values of 0.098 and 0.071 Ω cm^2 for 750 and 800 °C, respectively, which compares well with 0.115 and 0.069 Ω

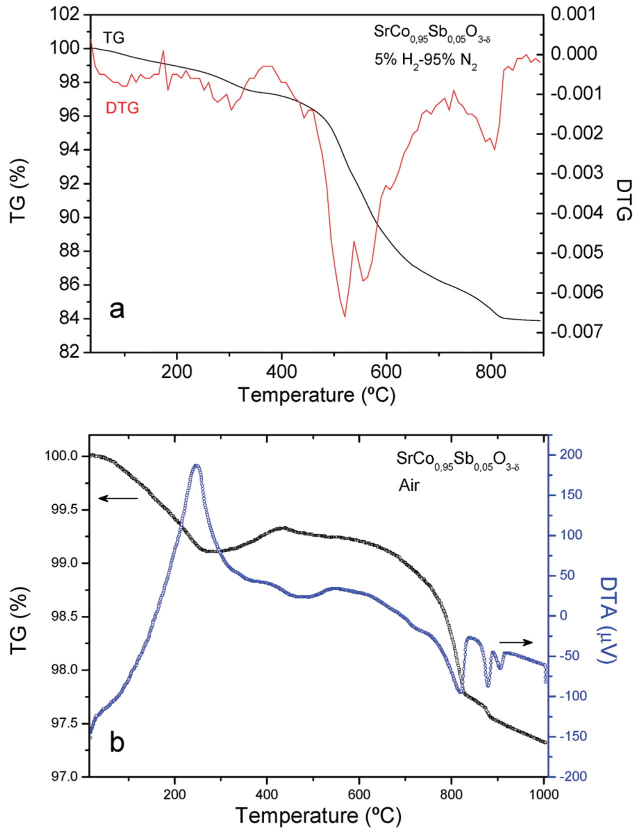

Figure 6. (a) Thermal analysis under reducing conditions (5% H_2:95% N_2) of $SrCo_{0.95}Sb_{0.05}O_{3-\delta}$;(b) thermal analysis curves recorded in air: TG (left axis) and DTA (right axis).

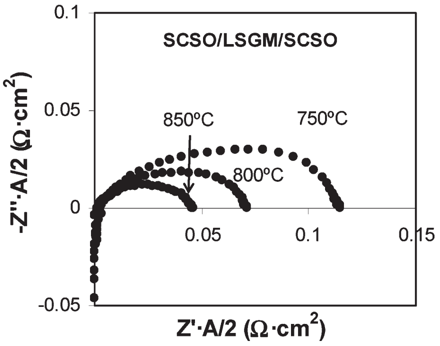

Figure 7. Impedance spectra obtained at 750, 800, and 850 °C in symmetrical cells of $SrCo_{0.95}Sb_{0.05}O_{3-\delta}$ over LSGM electrolyte.

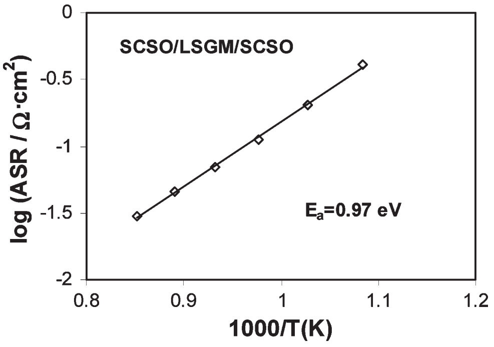

Figure 8. Arrhenius representation of the electrode polarization for $SrCo_{0.95}Sb_{0.05}O_{3-\delta}$.

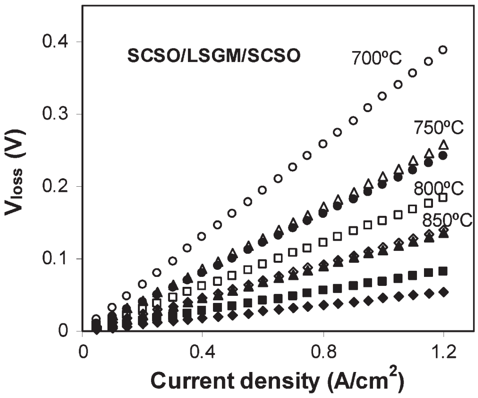

Figure 9. Voltage loss of the electrolyte (open symbols) and cathode overpotential (closed symbols) determined in a symmetrical cell of $SrCo_{0.95}Sb_{0.05}O_{3-\delta}$/LSGM/$SrCo_{0.95}Sb_{0.05}O_{3-\delta}$, at 700 (circles), 750 (triangles), 800 (squares), and 850 °C (diamonds).

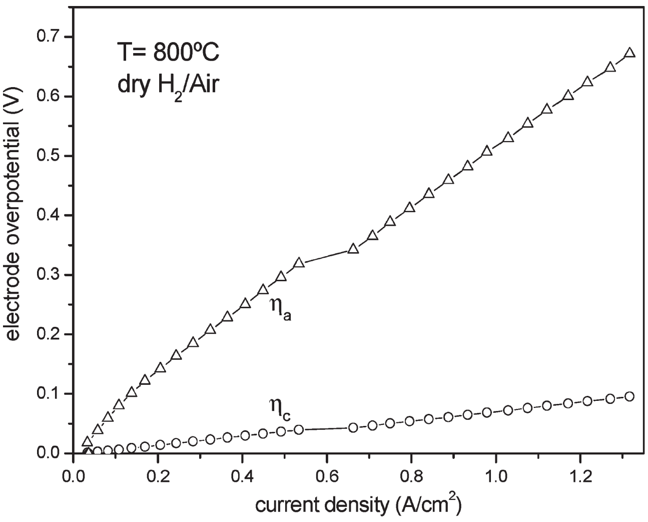

Figure 10. Anodic and cathodic overpotentials for test cells with Sr_2MgMoO_6 and $SrCo_{0.95}Sb_{0.05}O_{3-\delta}$ as anodic and cathodic materials.

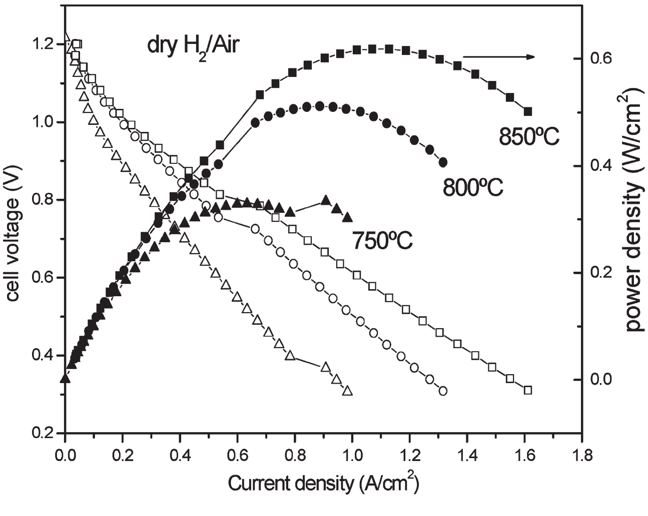

Figure 11. Cell voltage (left axis) and power density (right axis) as a function of the current density for the test cell with the configuration SMMO/ LDC/LSGM/SCSO.

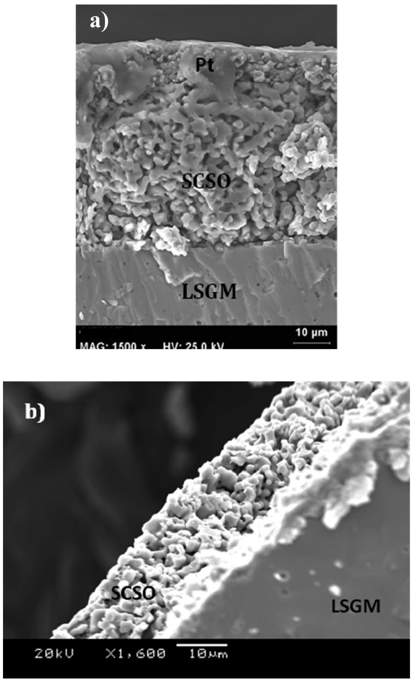

Figure 12. Cross-section SEM images of (a) the SCSO/LSGM/SCSO symmetrical cell and (b) the cathode side of the SMMO/ LDC/LSGM/ SCSO single cell.

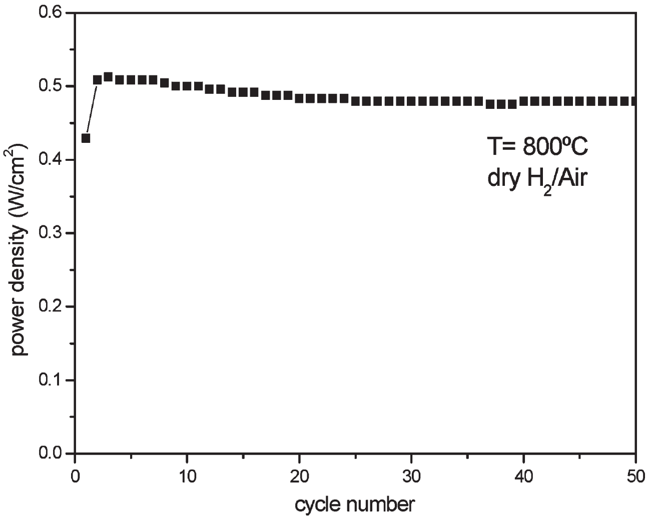

Figure 13. Stability of the test cell with $SrCo_{0.95}Sb_{0.05}O_{3-\delta}$ as cathodic material versus the cycle number.

cm^2 obtained by impedance spectroscopy. This test confirms the good performance of the cathode. Cross-section SEM images of the cathode-electrolyte interface reveals a good adherence and the absence of interdiffusion between the cathode and the electrolyte in both the single cell and the symmetrical cell measured (Figure 12).

Figure 13 shows the maximum power density at 800 °C obtained in 50 different cycles of fuel-cell test. The maximum power density starts with a value of 0.508 W cm^{-2}, and this value is retained for at least 7 cycles. Then there is a slight decrease in the value until 0.483 W cm^{-2} for the 20th cycle. For the following cycles, the maximum power density is approximately stable.

4. Discussion

The crystal structure of $SrCo_{0.95}Sb_{0.05}O_{3-\delta}$ in the temperature interval between 100 and 700 °C adopts a tetragonal superstructure of perovskite with a doubled a_0 axis along the *c* direction, as shown in Figure 4. Sb atoms are randomly distributed at Co2 positions, whereas Co1 sites do not apparently contain Sb. On the other hand, the oxygen vacancies are also ordered, in the sense that O1 is fully stoichiometric while the oxygen deficiency is concentrated on the O2 and O3 atoms, which belong to the coordination polyhedron of (Co,Sb)2. The (Co,Sb)2O_6 octahedra are elongated, with four (Co,Sb)2−-O3 bond lengths of 1.936 Å and two (Co,Sb)2−O2 bond-lengths of 2.104(3) Å at 100 °C; there is no significant evolution of this conformation in the 100−700 °C interval, apart from the expected thermal expansion and the fact that the octahedra become more regular as 700 °C is approached. By contrast, the Co1 octahedra are flattened along the *c* axial direction, displaying extremely short Co1−O2 distances of 1.794(3) Å at 100 °C. The four equivalent equatorial distances are 1.9361 Å at this temperature, and their thermal evolution follows the expected bond-length expansion. This long-range arrangement could be the origin of the observed superstructure along the *c* axis.

The oxygen stoichiometry in the tetragonal phase ranges from 2.72(4) at 100 °C to 2.64(5) at 700 °C, as shown in Figure 3c; accordingly, the average oxidation state for Co varies between 3.36+ and 3.19+, assuming a pentavalent oxidation state for Sb and divalent for Sr. There is a small but significant increase in the oxygen stoichiometry at 500 °C, which correlates well with the weight gain observed in the TG curve in the 300−430 °C range. It corresponds to an increase in the occupancy factors of both O2 and O3 oxygens. Also, there is a distinct contraction of the Co1−O2 and (Co,Sb)2−O2 bond lengths concomitant with the Co oxidation in this temperature interval. The crystal structure contains alternating small (Co1O_6) and large ((Co,Sb)2O_6) octahedra, with average ⟨(Co,Sb)−O⟩ distances of 1.889 and 1.992 Å at 100 °C and 1.924 and 2.014 Å at 700 °C, respectively. This fact suggests the establishment of a charge density wave (CDW) across both types of Co cations. Because the average valence for Co is 3.36+ at 100 °C, this hypothesis would imply an average oxidation state of $Co^{3.72+}$ at Co1 sites and Co^{3+} at (Co,Sb)2 positions, assuming a full charge disproportionation. In fact, the presence of intermediate spin Co^{3+} in (Co,Sb)2 sites would cause a Jahn−Teller elongation of the Co−O bond lengths, and the O^{2-} ions would preferentially bond with the Co^{4+} cations, to shift the O^{2-} ions from (Co,Sb)2 to Co1. Besides many metals and intermetallic alloys showing this effect, oxides are also known that stabilize a CDW and exhibit a high electronic conductivity, e.g., $LiVMoO_5$[32] or γ-Mo_4O_{11}.[33]

$SrCo_{0.95}Sb_{0.05}O_{3-\delta}$ experiences a phase transition from a tetragonal superstructure to a simple-cubic perovskite between 700 and 850 °C, probably associated with the endothermic peak observed at 816 °C in the DTA curve (Figure 6b). This phase transition is related to the disordering of the oxygen vacancies in the cubic unit cell with an average thermal factor and occupancy. Thus, the thermal factors for O1, O2, and O3 at 700 °C are, respectively, 3.0(1) Å^2, 3.9(4) Å^2 and 6.4(3) Å^2, merging into a single oxygen atom with an isotropic B factor of 4.8(1) Å^2 at 850 °C. The transition to a cubic phase at 800 °C mainly involves the disordering of the oxygen atoms in a cubic $Pm\overline{3}m$ subcell; we can assume that the Sb atoms are still long-range ordered, but their small amount (5% over the Co positions) precludes the observation of superstructure peaks and thus the unit cell is adequately described in a simple perovskite arystotype.

Once the sample has evolved from tetragonal to cubic, the total oxygen content refined from NPD data changes slightly from 2.50 atoms/f.u. at 850 °C to 2.46 atoms/f.u. at 930 °C, showing a progressive oxygen loss of the sample in equilibrium with an air atmosphere during the full NPD data acquisition. The total weight loss observed in the TG curve (Figure 5b) from 100 to 930 °C (0.29(1) oxygen atoms per formula) is in relatively good agreement with the difference in occupancy factors determined at both temperatures, of 0.24(3) oxygen atoms per formula. The behavior of the TG curve is not monotonous, showing a weight gain in the 300−430 °C interval, the onset of which correlates with the exothermic peak observed in the DTA curve at 260 °C, and the increment in the occupancy factor of O2 and O3 refined by neutron diffraction at 500 °C (Table 1). The possible temperature shifts between both techniques (TG and NPD) probably arise from the considerably more massive sample used in the neutron experiment, confined in a narrow quartz tube which may have delayed in some way the oxygen release/incorporation of the sample. From 700 °C the TG curve shows a more abrupt weight loss, which has also been observed in the in situ NPD study.

The electrical conductivity measurements were described for different compounds of the $SrCo_{1-x}Sb_xO_{3-\delta}$ series ($x = 0.05, 0.10, 0.15, 0.20$) [27] and a clear increment of the conductivity was observed with respect to the parent compound $SrCoO_{3-\delta}$, with a maximum conductivity for the present $x = 0.05$ sample reaching 500 S cm^{-1} at 400 °C. A further increment of the Sb content leads to a progressive decrease of the conductivity because the O−Sb−O bonds hinder the electronic mobility in the crystal. The thermal expansion of the $SrCo_{1-x}Sb_xO_{3-\delta}$ family was also previously reported for x = 0.05, 0.1, 0.15, 0.2; the absence of the abrupt anomalies found in the undoped compound should be noted. Even for the lowest Sb concentrations (x = 0.05), the thermal cracking problems that could be induced by the pristine sample $SrCoO_{3-\delta}$ have been overcome. However, the thermal expansion is not totally linear, showing an apparent change of slope at ∼400 °C, which could be identified with the oxygen incorporation and unit-cell contraction observed in this temperature regime.

The stabilization of a 3C superstructure of perovskite by the replacement of 5% Co by Sb in the parent $SrCoO_{3-\delta}$ perovskite is responsible for the observed performance

---

(32) Gopalakrishnan, J.; Bhuvanesh, N. S. P.; Vijayaraghavan, R.; Vasanthacharya, N. Y. *J. Mater. Chem.* **1997**, *7*, 307.

(33) Lope, E. B.; Almeida, M.; Dumas, J.; Guyot, H.; Escribe-Filippini, C. *J. Phys: Condens. Matter* **1992**, *4*, L357.

as a MIEC oxide, combining excellent ionic and electronic conductivity in the operating temperatures of an IT-SOFC. It is worth recalling that under similar preparation conditions, a material with starting $SrCoO_{3-\delta}$ stoichiometry would have produced a hexagonal 2H-like polytype containing face-sharing octahedra, the electrical properties of which are very poor below 900 °C.[34] We believe that the stabilization of a 3C perovskite structure with corner-sharing CoO_6 octahedra by the introduction of 5% Sb atoms relies on the presence of highly charged Sb^{5+} cations distributed at random over the B octahedral positions, preventing the highly repulsive conformations derived from the octahedral face-sharing involved in the hexagonal 2H polytypes. The introduction of Sb^{5+} cations also drives an electron-doping effect, enhancing a mixed valence over the Co cations and promoting the electrical conductivity.[27]

These structural features account for the successful use of $SrCo_{0.95}Sb_{0.05}O_{3-\delta}$ as cathode material in single test cells with pure H_2 as a fuel, displaying maximum output powers of 0.328, 0.511, and 0.618 W/cm^2 for temperatures of 750, 800, and 850 °C, respectively, surpassing the practical requirements of 500 mW/cm^2 at 800 °C for a single cell. It also exhibits a good cyclability without apparent power loss up to 50 cycles. The cathodic overpotential is significantly smaller than the anodic one, and therefore the cathodic losses are no longer rate-determining of the output power of the cell. Moreover, the cathodic overpotential matches well with the electrode polarization resistance obtained by impedance spectroscopy in air, giving values below 0.1 Ω cm^2 for 750 and 800 °C.

5. Conclusions

We have designed, characterized and tested defective Sb-doped derivatives of the $SrCoO_{3-\delta}$ perovskite as cathode materials for intermediate-temperature SOFCs with long-term stability and competitive power performance in the temperature range 750−850 °C. In particular, $SrCo_{0.95}Sb_{0.05}O_{3-\delta}$ features a number of interesting properties that account for the observed performance: it presents a maximum electronic conductivity, as high as 500 S cm^{-1} at 400 °C, and low electrode polarization resistance with the LSGM electrolyte, below 0.1 Ω cm^2 in the 750−800 °C range; the crystal structure adopts a 3C corner-linked perovskite network with a considerable number of oxygen vacancies, the oxygen atoms showing high thermal factors (4−6 Å^2 in the 700−850 °C range) suggesting a significant ionic mobility. The low-temperature tetragonal superstructure undergoes a smooth transition to a completely disordered cubic structure in the temperature range 700 to 850 °C, probably at 816 °C from the DTA curve. This structure is stable up to 930 °C; at this temperature the oxygen stoichiometry is 2.46(4). The stabilization of a 3C perovskite structure with corner-sharing CoO_6 octahedra by the introduction of 5% Sb atoms relies on the presence of highly charged Sb^{5+} cations distributed over the B octahedral positions, preventing the highly repulsive conformations derived from the face-sharing octahedra of the hexagonal 2H polytypes, which are characterized by a low electronic conductivity and present unwanted reconstructive phase transitions in the useful temperature regime of SOFCs.

Acknowledgment. We are grateful to ILL for making the beamtime available. J.B.G. thanks the NSF and the Robert A. Welch Foundation of Houston, TX, Grant #F-1066, for financial support. A.A., C.C., and J.A.A. acknowledge the financial support of the Spanish “Ministerio de Ciencia e Innovación” (MICINN) to the Project MAT2007-60536; J.A.A. is grateful to MICINN for support during his sabbatical. A.A. and D.P.C. wish to thank to MICINN for a “Juan de la Cierva” and a “Ramón y Cajal” contracts, respectively.

---

[34] Deng, Z. Q.; Yang, W. S.; Liu, W.; Chen, C. S. *J. Solid State Chem.* **2006**, *179*, 362.